Subspace variational quantum simulator

Kentaro Heya,[1,*] Ken M. Nakanishi,[2] Kosuke Mitarai,[3,4,5] Zhiguang Yan,[1] Kun Zuo,[1] Yasunari Suzuki,[6,5] Takanori Sugiyama,[7] Shuhei Tamate,[1] Yutaka Tabuchi,[1] Keisuke Fujii,[3,4,1] and Yasunobu Nakamura[8,1]

[1]*RIKEN Center for Quantum Computing (RQC), Wako, Saitama 351-0198, Japan*
[2]*Institute for Physics of Intelligence, The University of Tokyo, Tokyo 113-0033, Japan*
[3]*Graduate School of Engineering Science, Osaka University, 1-3 Machikaneyama, Toyonaka, Osaka 560-8531, Japan*
[4]*Center for Quantum Information and Quantum Biology, Osaka University, Japan*
[5]*JST, PRESTO, 4-1-8 Honcho, Kawaguchi, Saitama 332-0012, Japan*
[6]*NTT Computer and Data Science Laboratories, NTT Corporation, Musashino 180-8585, Japan*
[7]*Research Center for Advanced Science and Technology (RCAST), The University of Tokyo, Meguro-ku, Tokyo 153-8904, Japan*
[8]*Department of Applied Physics, Graduate School of Engineering, The University of Tokyo, Bunkyo-ku, Tokyo 113-8656, Japan*

(Received 1 June 2022; accepted 29 March 2023; published 1 May 2023)

Quantum simulation is one of the key applications of quantum computing, which accelerates research and development in the fields such as chemistry and material science. The recent development of noisy intermediate-scale quantum (NISQ) devices urges the exploration of applications without the necessity of quantum error correction. In this paper, we propose an efficient method to simulate quantum dynamics driven by a static Hamiltonian on NISQ devices, named subspace variational quantum simulator (SVQS). SVQS employs the subspace-search variational quantum eigensolver (SSVQE) [Phys. Rev. Res. **1**, 033062 (2019)] to find a low-lying eigensubspace and extends it to simulate dynamics within the subspace with lower overhead compared to the existing schemes. We experimentally simulate the time-evolution operator in a low-lying eigensubspace of a hydrogen molecule. We also define the subspace process fidelity as a measure between two quantum processes in a subspace. The subspace time evolution mimicked by SVQS shows the subspace process fidelity of 0.896–0.989.

DOI: 10.1103/PhysRevResearch.5.023078

I. INTRODUCTION

The dynamical properties of quantum systems are of great scientific interest and practically important for applications, and hence researchers have developed classical simulation algorithms such as the time-dependent density functional theory [1]. A controllable quantum system must be advantageous in simulating such dynamics over a classical computer [2]. Simulations of quantum dynamics have been intensively studied as one of the most promising applications of quantum computers [3].

Methods for simulating quantum dynamics on a quantum computer were first proposed based on Trotterization [4–6] and have been extended by incorporating linear combinations of unitaries [7,8], truncated Dyson series [9], quantum random walk [10,11], and quantum signal processing [12]. While these methods are based on rigorous algorithms with error guarantees, they run only on a fault-tolerant quantum computer and are not tolerant to device-specific errors without error correction. The required circuits are also too deep to demonstrate their performance on the present NISQ devices. While this problem is expected to be overcome in future by quantum error correction [13,14], assessment of the computational power of NISQ devices is also of great interest [15–17].

A suitable approach for NISQ devices is quantum–classical hybrid algorithms that utilize a variational method and shallow parameterized quantum circuits [18]. These algorithms, such as variational quantum eigensolvers [19–22], generally do not guarantee the accuracy of solutions but can be feasibly implemented on NISQ devices. Simulations of quantum dynamics in the framework of quantum–classical hybrid algorithms originated in variational quantum simulation (VQS) [23–26]. VQS approximates an arbitrary time evolution within the representational capability of a parameterized quantum circuit by updating the variational parameters of the circuit at each time step according to the time-dependent variational principle. While VQS applies to the simulation of time-dependent Hamiltonian dynamics, it requires experiments using ancilla qubits and controlled operations to update the variational parameters at each time step. An easier way to solve the time-independent Hamiltonian dynamics without such an iterative procedure is to diagonalize the given Hamiltonian. From the basis transformation matrix and eigenvalues obtained by diagonalization, the time-evolution operator can be easily reproduced. However, diagonalizing a high-dimensional Hamiltonian generally requires the execution of a quantum circuit too deep for NISQ devices.

*kheya@qc.rcast.u-tokyo.ac.jp

Several hybrid quantum–classical algorithms have been proposed to solve time-independent Hamiltonian dynamics on NISQ devices [8,27–30]. A representative method is the so-called variational fast-forwarding (VFF) [27,30]. In VFF, one first trains a parameterized quantum circuit to mimic the short time-evolution operator and then extrapolates the time evolution by updating the variational parameters, without calling for additional quantum experiments. VFF fully approximates the time-evolution operator with a parameterized quantum circuit, which is as difficult as quantum optimal control with a large number of qubits.

In this paper, we propose a quantum–classical hybrid algorithm for efficiently simulating time-independent Hamiltonian dynamics and experimentally demonstrate it on superconducting qubits. The method, named subspace variational quantum simulator (SVQS), avoids the difficulties of Hamiltonian diagonalization described above by restricting itself to partial diagonalization. First, we use subspace-search variational quantum eigensolver (SSVQE) [31], one of the methods for partially diagonalizing only a low-lying eigensubspace of the Hamiltonian $\mathcal{H}$ [32–34]. In SSVQE, we find a unitary $U(\boldsymbol{\theta}^*)$ that maps k orthogonal input states $\{|\varphi_i\rangle\}_{i=1}^k$ chosen from the computational basis to the excited states up to the kth $\{|E_i\rangle\}_{i=1}^k$, each having the corresponding eigenenergy E_i. It is expected that the representation capability of the parameterized quantum circuit required for a partial diagonalization of the Hamiltonian is much lower than that for the full diagonalization, and can be realized in a shallower circuit. In SVQS, the inverse of the unitary, $U^\dagger(\boldsymbol{\theta}^*)$, maps each $|E_i\rangle$ to a computational basis $|\varphi_i\rangle$, where we can easily apply phase factors e^{-iE_it}. Unlike VFF, SVQS mimics the time-evolution operator only for states in a specific eigensubspace. However, it is expected that the cost required for training parameterized quantum circuits is lower than VFF. SVQS and VFF have a trade-off between the size of the simulatable eigensubspace and the easiness of the implementation, and thus are complementary with each other.

The rest of this paper is organized as follows. In Sec. II, we describe the method of SVQS in detail. In Sec. III, we demonstrate SSVQE and SVQS on a system with two superconducting transmon qubits to simulate quantum dynamics of a hydrogen molecule. To characterize the subspace time evolution mimicked by SVQS, we define the subspace process fidelity as a measure between two quantum processes in a subspace. Even with the limited device performance, the subspace time evolution in the low-lying eigensubspace of a hydrogen molecule mimicked by SVQS shows the subspace process fidelity of 0.896–0.989. SVQS is effective for experiments on NISQ devices because of the modest requirement for experimental devices.

II. METHODS

In this section, we first introduce the subspace-search variational quantum eigensolver (SSVQE) [31], which is the key ingredient for our proposal. We then describe our proposal, the subspace variational quantum simulator (SVQS). In the following subsections, $\mathcal{H}$ denotes a n-qubit Hamiltonian transformed from the given Hamiltonian as follows:

$$\mathcal{H} = \sum_{j=1}^{2^n} E_j \, |E_j\rangle \, \langle E_j| \, , \tag{1}$$

where E_j and $|E_j\rangle$ are the jth eigenenergy and eigenstate of $\mathcal{H}$, respectively. In applications for quantum chemistry, Jordan-Wigner [35] or Bravyi-Kitaev [36] transformation can be utilized to map a fermionic Hamiltonian to an n-qubit Hamiltonian.

A. Subspace-search variational quantum eigensolver

SSVQE is an algorithm for finding the kth or up to the kth excited states of Hamiltonian $\mathcal{H}$ [31]. To find excited states up to the kth, SSVQE takes k orthogonal states as inputs of a parameterized quantum circuit and minimizes the weighted sum of the expected energies of the output states. The output states become automatically an orthogonal set by the conservation of orthogonality under the unitary transformation. Therefore, we find all the excited states up to the kth via a single optimization procedure. The procedure of SSVQE is summarized as follows:

(1) Construct a parameterized quantum circuit $U(\boldsymbol{\theta})$ and prepare k initial states $\{|\varphi_j\rangle\}_{j=0}^k$ $(k \leqslant 2^n)$, which are orthogonal to each other $(\langle\varphi_i|\varphi_j\rangle = \delta_{i,j})$.

(2) Minimize $\mathcal{L}_{\boldsymbol{\omega}}(\boldsymbol{\theta}) = \sum_{j=0}^k \omega_j \, \langle\varphi_j|U^\dagger(\boldsymbol{\theta})\mathcal{H}U(\boldsymbol{\theta})|\varphi_j\rangle$, where the weight vector $\boldsymbol{\omega}$ is chosen such that $\omega_i > \omega_j$ when $i < j$.

Successfully optimizing $\boldsymbol{\theta}$ of an appropriate parameterized quantum circuit $U(\boldsymbol{\theta})$ by the procedure above, each output state $|\psi_j(\boldsymbol{\theta})\rangle \equiv U(\boldsymbol{\theta})\,|\varphi_j\rangle$ $(j = 0, 1, \ldots, k)$ converges to the following state:

$$|\psi_j(\boldsymbol{\theta}^*)\rangle = e^{i\delta_j} \, |E_j\rangle \, , \tag{2}$$

where δ_j is an unknown global phase factor, and $\boldsymbol{\theta}^*$ denotes the parameters that minimizes $\mathcal{L}_{\boldsymbol{\omega}}(\boldsymbol{\theta})$. Therefore, the obtained circuit $U(\boldsymbol{\theta}^*)$ corresponds to a map between the computational subspace $\mathcal{S}_{\rm com}$ spanned by the orthogonal initial states $\{|\varphi_j\rangle\}_{j=1}^k$ and the eigensubspace $\mathcal{S}_\parallel$ spanned by the excited states $\{|E_j\rangle\}_{j=1}^k$.

B. Subspace variational quantum simulator

The key idea of SVQS is to map a low-lying eigensubspace $\mathcal{S}_\parallel$ of the target Hamiltonian $\mathcal{H}$ to a computational subspace $\mathcal{S}_{\rm com}$ spanned by the orthogonal initial states specified in SSVQE. The procedure of the SVQS is summarized as follows:

(1) Construct a parameterized quantum circuit $U(\boldsymbol{\theta})$ and prepare l input states $\{|\varphi_j\rangle \,|\, |\varphi_j\rangle = X_j\,|0\rangle^{\otimes n}\}_{j=1}^l$ $(l \leqslant n)$ such that they are orthogonal to each other $(\langle\varphi_j|\varphi_{j'}\rangle = \delta_{j,j'})$.

(2) Minimize $\mathcal{L}_{\boldsymbol{\omega}}(\boldsymbol{\theta}) = \sum_{j=1}^l \omega_j \, \langle\varphi_j|U^\dagger(\boldsymbol{\theta})\mathcal{H}U(\boldsymbol{\theta})|\varphi_j\rangle$, where the weight vector $\boldsymbol{\omega}$ is chosen such that $\omega_i > \omega_j$ when $i < j$.

(3) After convergence, get the jth eigenenergy E_j as $\langle\varphi_j|\,U^\dagger(\boldsymbol{\theta}^*)\mathcal{H}U(\boldsymbol{\theta}^*)\,|\varphi_j\rangle$ with the converged variational parameter $\boldsymbol{\theta}^* = \arg\min\mathcal{L}_{\boldsymbol{\omega}}(\boldsymbol{\theta})$.

(4) Prepare an initial state $|\psi_{\rm in}\rangle$ in the eigensubspace $\mathcal{S}_\parallel$.

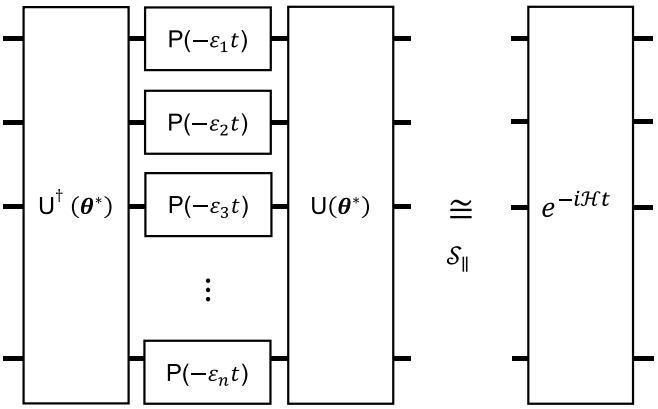

FIG. 1. Quantum circuit for SVQS. $P(\xi)$ denotes a phase gate with the rotation angle ξ. The quantum circuit shown on the left approximates the time-evolution operator within the eigensubspace $\mathcal{S}_\parallel$.

(5) Encode the input state $|\psi_{\text{in}}\rangle$ on the eigensubspace $\mathcal{S}_\parallel$ into the computational subspace $\mathcal{S}_{\text{com}}$ by applying the Hermitian conjugate of the obtained circuit $U^\dagger(\boldsymbol{\theta}^*)$.

(6) Apply a single-qubit phase-rotation on each qubit, namely, $V(t) = \bigotimes_{j=1}^{l} P(-E_j t)$, where $P(\xi) = |0\rangle\langle 0| + e^{i\xi}|1\rangle\langle 1|$ is a phase gate.

(7) Decode the state $V(t)U^\dagger(\boldsymbol{\theta}^*)|\psi_{\text{in}}\rangle$ on the computational subspace $\mathcal{S}_{\text{com}}$ into the eigensubspace $\mathcal{S}_\parallel$ by applying $U(\boldsymbol{\theta}^*)$. See also Fig. 1 showing the quantum circuit corresponding to steps 4–6 of the procedure.

Let us explain how the above procedure works to simulate the time evolution of a quantum system. The circuit $U(\boldsymbol{\theta}^*)$ obtained in step 2 corresponds to a map between $\mathcal{S}_\parallel$ and $\mathcal{S}_{\text{com}}$. Therefore, the circuit $U(\boldsymbol{\theta}^*)$ can be denoted as follows:

$$U(\boldsymbol{\theta}^*) = \sum_j e^{i\delta_j} |E_j\rangle\langle\varphi_j| + U_\perp, \tag{3}$$

where $\{\delta_j\}_{j=1}^{l}$ are unknown phase offsets and $U_\perp$ is an unknown map between the subspaces complementary to $\mathcal{S}_\parallel$ and $\mathcal{S}_{\text{com}}$. The unknown phase offset occurs due to the nature of SSVQE only evaluating the energy values. This offset makes phase synchronization between the computational basis and eigenbasis difficult. However, we can cancel this offset by utilizing the inversed parameterized quantum circuit, as described below. The tensor product of the single-qubit phase rotations can be denoted as follows:

$$V(t) = \sum_{j=1}^{l} e^{-iE_j t} |\varphi_j\rangle\langle\varphi_j| + U'_\perp(t), \tag{4}$$

where $U'_\perp(t)$ is again a map between the complementary subspaces. Under the conjugation by Eqs. (3) and (4) transforms as follows:

$$\mathcal{T}(t) = U(\boldsymbol{\theta}^*)V(t)U^\dagger(\boldsymbol{\theta}^*) \tag{5}$$

$$= \sum_{j=1}^{l} e^{-iE_j t} |E_j\rangle\langle E_j| + U_\perp U'_\perp(t) U_\perp^\dagger. \tag{6}$$

Equation (5) corresponds to the subspace time-evolution operator on the l-dimentional eigensubspace with an unknown time-dependent unitary operation on the complementary subspace. The single-qubit phase rotations can be implemented with high-fidelity virtual Z gates [37]. Note that if we could know the expansion coefficients of the initial state on the eigenbasis efficiently, we could classically simulate the time evolution for the state by using the eigenenergies obtained in SSVQE. However, it is generally hard to run state tomography for eigenstates with many qubits. SVQS does not require state tomography of eigenstates, and can directly generate a time-evolution operator on a quantum circuit.

C. Extensions of SVQS

In this subsection, we propose extensions for SVQS. The first extension is a method to extend the dimension of the simulatable eigensubspace $\mathcal{S}_\parallel$. In Sec. II B, for a n-qubit target Hamiltonian, the dimension of the simulatable eigensubspace restricts to n, because there only exist n one-hot states in the n-qubit system. In this extension, we introduce a-ancilla qubits to extend the dimension of the simulatable eigensubspace to $n + a$. The Hamiltonian of the $(n + a)$-qubit system is defined in terms of n-qubit Hamiltonian $\mathcal{H}_n$ as follows:

$$\mathcal{H} = \mathcal{H}_n \otimes I_a - E_{\text{B}} I_n \otimes \sum_{i=1}^{a} (I_i - Z_i), \tag{7}$$

where $I_{n,a}$ denote the identity operators for n- and a-qubit subspace, and I_i and Z_i denote the identity and Pauli-Z operators on the ith ancilla qubit, and E_{B} is an energy constant much larger than the $(n + a)$th excited-state eigenenergy. The first term of the target Hamiltonian corresponds to the problem Hamiltonian on the n-qubit system, and the second term corresponds to the static energy bias E_{B} applied to the ancilla qubits. If the energy bias E_{B} is larger than the eigenenergy of the $(n + a)$th excited eigenstate of the problem Hamiltonian, then the ith excited eigenstate of the total Hamiltonian becomes

$$|\psi^i\rangle = |\psi_n^i\rangle \otimes |0\rangle^{\otimes a}, \tag{8}$$

where $|\psi_n^i\rangle$ denotes the ith excited eigenstate of the n-qubit Hamiltonian $\mathcal{H}_n$. Note that such a method does not disturb the low-lying eigenstates or eigenenergies of the problem Hamiltonian. Therefore, by running SVQS with n data qubits and a ancilla qubit, we can search up to the $(n + a)$th excited state of the n-qubit Hamiltonian.

The second extension is controlled-SVQS. By replacing the phase gates in the quantum circuits drawn in Fig. 1 with controlled phase gates, the subspace time evolution obtained with SVQS can easily be extended to the controlled subspace time evolution. Simulation of the controlled time evolution is useful for calculating the generalized Green functions [38,39], out-of-time-order correlations [40], and Loschmidt echo signals [41].

III. EXPERIMENT

A. System

Here, we demonstrate SVQS using two superconducting qubits (Q0 and Q1) capacitively coupled with each other. The

TABLE I. Parameters of the two superconducting transmon qubits (Q0 and Q1) used in the experiments: the qubit frequency ω_q, anharmonicity α, relaxation time T_1, and echo dephasing time T_2^{echo}.

	$\omega_q/2\pi$ (GHz)	$\alpha/2\pi$ (MHz)	T_1 (μs)	T_2^{echo} (μs)
Q0	8.209	−380	4.3	8.9
Q1	8.965	−410	4.6	6.5

qubits are a part of a 16-qubit device [42]. The parameters of the qubits are summarized in Table I. The static ZZ interaction strength between the qubits is −230 kHz.

We calibrate and implement single-qubit gates, $R_Z(\theta) = e^{-i\frac{\theta}{2}Z}$ and $R_X(\pi/2) = e^{-i\frac{\pi}{4}X}$, and a two-qubit gate $R_{ZX}(\pi/4) = e^{-i\frac{\pi}{8}ZX}$. The $R_Z(\theta)$ gates are implemented with the virtual Z gates [37]. The $R_X(\pi/2)$ gates are implemented with the shaped microwave pulse [43] with the total duration of 13.9 ns for Q0 and 14.1 ns for Q1. The averaged gate fidelities of the single-qubit Clifford gates are 0.9974(4) and 0.9958(5) via the simultaneous randomized benchmarking [44], where the coherence limits of both qubits are 0.998. The $R_{ZX}(\pi/4)$ gates are implemented with a cross-resonance gate [45,46] with the total duration of 73.3 ns. The averaged gate fidelity of the $R_{ZX}(\pi/2)$ gate is determined to be 0.963(4) via the interleaved randomized benchmarking [47], where the coherence limit is 0.961. The experimental results of the randomized benchmarking are shown in Fig. 2.

The multiplexed single-shot dispersive readout of the qubits [49,50] are performed via readout resonators at 10.119 and 10.341 GHz for Q0 and Q1, respectively, and a common Purcell filter [51,52]. The readout signal is amplified with an impedance-matched Josephson parametric amplifier [53,54]. The thermal populations of the qubits in equilibrium are 7.84% and 11.72%. The assignment fidelities of the single-shot readout are 0.946 and 0.922, respectively.

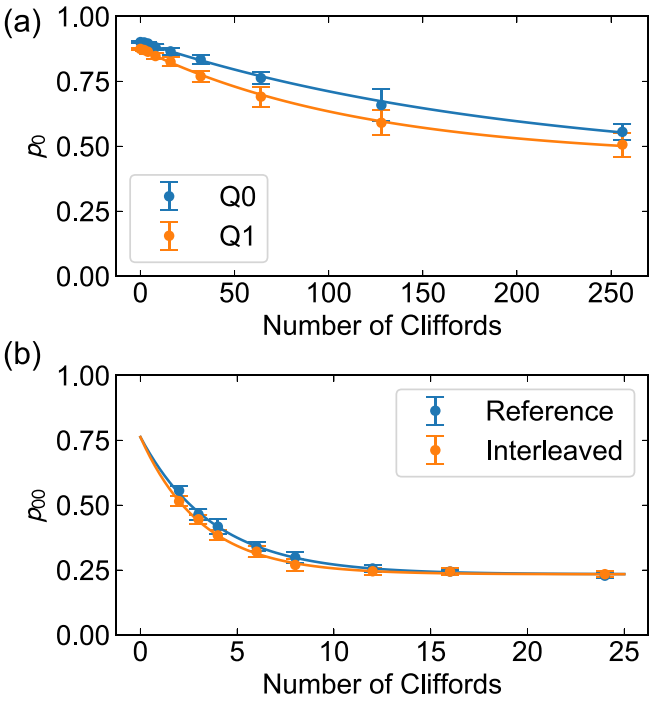

FIG. 2. Experimental results of (a) the single-qubit simultaneous randomized benchmarking and (b) the two-qubit interleaved randomized benchmarking. To align the execution times of all the Clifford gates, the single-qubit and two-qubit Clifford gates are constructed based on Euler decomposition [37] and KAK decomposition [48], respectively. Therefore, each single-qubit Clifford gate is implemented with two $R_X(\pi/2)$ and three $R_Z(\theta)$ gates, and each two-qubit Clifford gate is implemented with 28 $R_X(\pi/2)$, 27 $R_Z(\theta)$, and 6 $R_{ZX}(\pi/4)$ gates except the ones for the interleaved $R_{ZX}(\pi/2)$ gates. We take 10 random circuits for each Clifford sequence length and have 10^4 sampling of measurements for each random circuit to obtain a single data point. The ground-state populations of each qubit p_0 and two qubits p_{00} are fitted to the exponential decay.

B. Subspace-search variational quantum eigensolver

First, we demonstrate SSVQE. The Hamiltonian of a hydrogen molecule in STO-3G basis can be converted into a two-qubit Hamiltonian [55] as follows:

$$\mathcal{H} = c_0 II + c_1 ZI + c_2 IZ + c_3 XX + c_4 YY + c_5 ZZ, \quad (9)$$

where the coefficients c_i are calculated with openfermion [56] and Psi4 [57]. In the following experiments, we use a minimal clique cover [58–62] to reduce the number of experiments required for the evaluation of the expectation values of the Hamiltonian.

In the optimization protocol, we employ the hardware-efficient ansatz $U(\boldsymbol{\theta})$ with 18 parameters shown in Fig. 3(a). We optimize the parameterized quantum circuit on our experimental system to incorporate the system imperfection with the initial parameters given by the numerical simulation. We prepare the initial states $|\varphi_j\rangle$ by thermalizing the qubits to the environment at a sufficiently low temperature (∼10 mK) for a sufficiently longer time than the energy relaxation time and then performing an X-gate on the jth qubit. Then, we operate the parameterized quantum circuit and evaluate the energy expectation values for the final states. Finally, we calculate the cost function by taking the linear sum of the energy expectation values for the final states with the weighting factors $\omega_0 = 2$ and $\omega_1 = 1$.

To minimize the effect of imperfections in the circuit, we use gate-error mitigation [23,63,64] and measurement-error mitigation [64–67]. The former is a method to estimate the measurement results for the ideal case without gate errors by the linear extrapolation of experimental results obtained for different gate execution times. The latter is a method to estimate the ideal measurement results in the absence of measurement errors by using a predetermined measurement confusion matrix. We run the experimental SSVQE with 36 iterations. Both in the numerical and experimental SSVQEs, we adopt the sequential minimal optimization method [68] as the optimizer.

Figure 4 shows the experimental results of the SSVQE for different atomic distances, where the evaluated eigenenergies match well to the theoretical values within ±0.1 h/Ha. The details of the optimization procedures are shown in Appendix A.

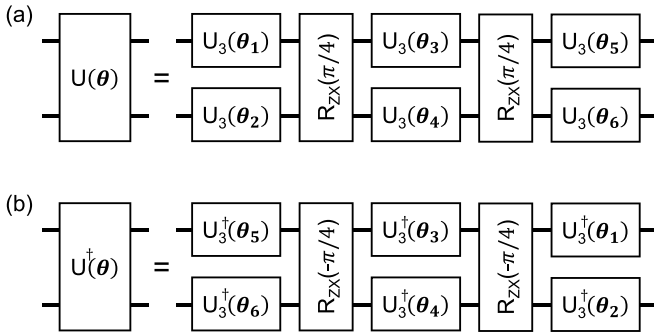

FIG. 3. (a) Hardware efficient ansatz used in the SSVQE experiments and (b) its Hermitian conjugate used in the SVQS experiments, where $U_3(\boldsymbol{\theta})$ ($\boldsymbol{\theta} = \{\boldsymbol{\theta}_i\}$; $i = 1, \ldots, 6$) represents a parameterized single-qubit rotation implemented with two $R_X(\pi/2)$ gates and three parameterized R_Z gates [37]. Each $\boldsymbol{\theta}_i$ consists of three phase parameters.

C. Subspace variational quantum simulator

Next, we demonstrate SVQS. In the following experiments, the atomic distance is set to 1.0 Å, for simplicity.

As discussed in Sec. II B, the subspace time-evolution operator for the low-lying eigensubspace $\mathcal{S}_\parallel$ can be systematically implemented with the quantum circuit drawn in Fig. 1, where $U(\boldsymbol{\theta}^*)$ obtained from SSVQE [Fig. 3(a)] and its Hermitian conjugate $U^\dagger(\boldsymbol{\theta}^*)$ [Fig. 3(b)] are used.

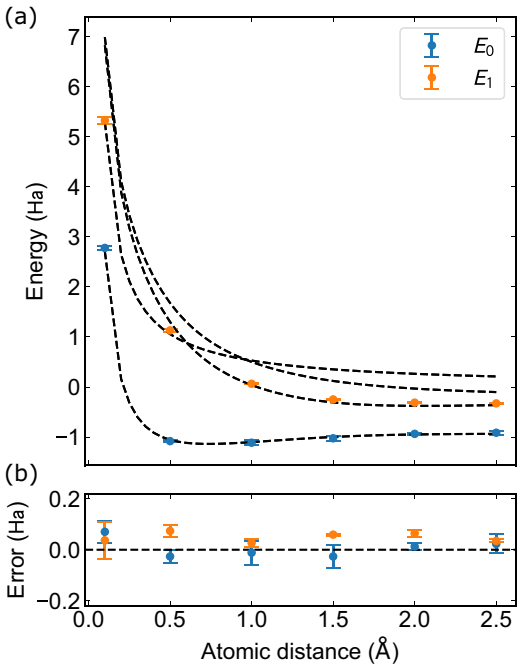

FIG. 4. SSVQE for different atomic distances. Panels (a) and (b) show the eigenergies and residual errors at the convergence points, respectively. The blue and orange dots represent the experimentally obtained ground and first-excited eigenenergies, respectively. The error bars indicate the standard deviation of the eigenenergies, where the shot number is 10^4. In panel (a), the black dashed lines depict the theoretical eigenenergies of the hydrogen molecule.

We perform quantum process tomography [69] for the subspace time-evolution operators mimicked by SVQS, where we apply the gate-error mitigation and the measurement-error mitigation. To estimate the quantum processes, we use Quara [70], a software package for quantum characterization. In Quara, quantum processes are estimated with the maximum likelihood method under a predetermined measurement confusion matrix. We sweep the evolution time from 0 to 5.4 h/Ha, which roughly corresponds to one cycle of the time evolution, $T = 2\pi/(E_1 - E_0)$, in the low-lying eigensubspace.

To properly evaluate the performance of the time evolution mimicked by SVQS, we introduce the subspace Pauli transfer matrix (SPTM) and the subspace process infidelity (SPIF) as a representation and error measure of the quantum processes in a subspace, respectively. SPTM and SPIF are natural derivatives of Pauli transfer matrix and process infidelity used for quantum processes in the whole space, respectively. The details of the definition of SPTM and SPIF are described in Appendix B. Figure 5 shows the experimental results of SVQS. Figure 5(a) shows the ideal and experimental SPTMs of the subspace-time evolution operators mimicked by SVQS while sweeping the evolution time. The SPTMs show that the time evolution mimicked by SVQS corresponds to the subspace Pauli-Z rotation and is in good agreement with the ideal time evolution. Figure 5(b) shows the experimental SPIF of the subspace-time evolution operators. The SPIF takes values of 0.011–0.104. In the two-dimensional low-lying eigensubspace, subspace time evolution corresponds to a rotating operation in SO(3). A detailed analysis in Appendix C reveals the subspace time evolution corresponding to a 1.1% speed error and a 19.3° axis error in the rotating operation.

IV. CONCLUSION

In this paper, we proposed an efficient algorithm, subspace variational quantum simulator (SVQS), to simulate quantum dynamics on a NISQ device. The circuit depth required in SVQS is at most twice as large as that of the subspace-search variational quantum eigensolver (SSVQE) on the same device. Recently, there have been proposals to implement VQE for larger-scale quantum systems [71–75]. It is expected that SVQS can also be implemented for larger-scale systems.

We experimentally demonstrated SVQS using a system consisting of two superconducting qubits. Even with the limited device performance, we approximated the quantum dynamics in the two-dimensional low-lying eigensubspace of a hydrogen molecule with subspace process fidelity of 0.896–0.989. This suggests that our proposal is effective for experiments on NISQ devices because of the modest requirements for experimental devices.

In SVQS, we apply the parameterized quantum circuit obtained with SSVQE as a map between a low-lying eigensubspace and a computational subspace and implement subspace time evolution as phase rotations on the eigenbasis. The relationship between SSVQE, which gives the desired map, and SVQS, which utilizes the map, is similar to the relationship between quantum phase estimation [76–78] and HHL algorithm [79]. The similarity suggests a possible path toward

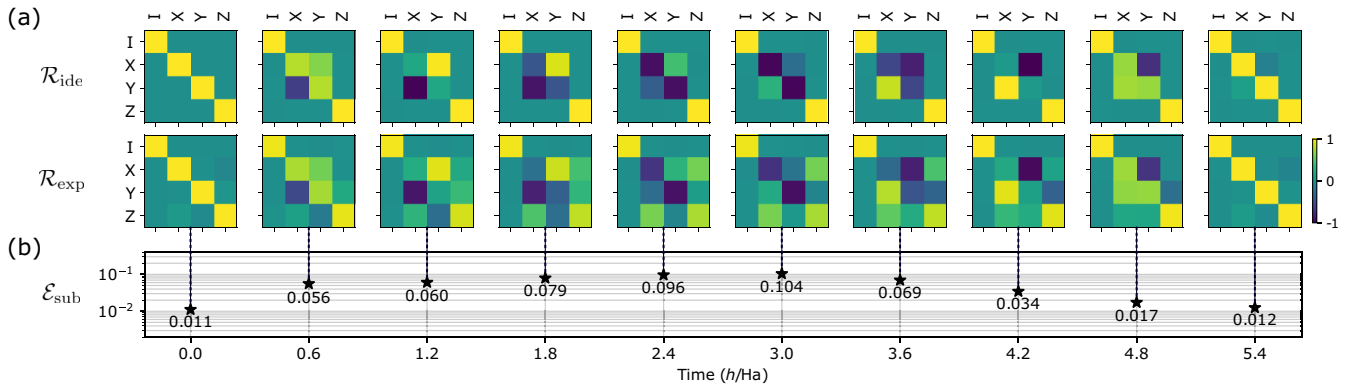

FIG. 5. SVQS for the evolution time from 0 to 5.4 h/Ha. (a) Ideal and experimental subspace Pauli transfer matrices, $\mathcal{R}_{\rm ide}$ (top) and $\mathcal{R}_{\rm exp}$ (bottom), of the subspace time-evolution operators in the low-lying eigensubspace $\mathcal{S}_{\|}$ for the evolution time $t = 0$ to 5.4 h/Ha. (b) Subspace process infidelity $\mathcal{E}_{\rm sub}$ between the ideal and experimental subspace time-evolution operators. The details are found in Appendix C.

hybrid quantum–classical algorithms that can be applied to a wider range of problems including linear equations.

The data that support the findings of this study are available from the corresponding authors upon reasonable request.

The code that is deemed central to the conclusions are available from the corresponding author upon reasonable request.

ACKNOWLEDGMENTS

This work was supported by QunaSys. K.H., K.M.N., and K.M. thank IPA for its support through MITOU Target program. K.H. was supported by JSPS KAKENHI (Grant No. JP21J15221). K.M.N. was supported by JSPS KAKENHI (Grant No. JP20J13955), and the Daikin Endowed Research Unit: "Research on Physics of Intelligence," School of Science, the University of Tokyo. K.M. was supported by JST PRESTO (Grant No. JPMJPR2019) and JSPS KAKENHI (Grant No. JP20K22330). K.F. was supported by JSPS KAKENHI (Grant No. JP16H02211), JST ERATO (Grant No. JPMJER1601), JST CREST (Grant No. JPMJCR1673), and MEXT Q-LEAP (Grant No. JPMXS0120319794). Y.S. was supported by JST PRESTO (Grant No. JPMJPR1916) and JST Moonshot R&D (Grant No. JPMJMS2061). K.H., Y.S., Z.Y., K.Z., T.S., S.T., Y.T., and Y.N. were partly supported by JST ERATO (Grant No. JPMJER1601) and by MEXT Q-LEAP (Grant No. JPMXS0118068682).

K.H. designed the theoretial concepts. K.H. designed and performed the experiments. K.M.N. designed the SVQS extensions using ancilla qubits. S.T. and Y.T. designed the device and the control system. Z.Y. and K.Z. designed and calibrated the impedance-matched Josephson parametric amplifier. K.H. performed the numerical and analytical calculations. K.H., Y.S., and T.S., analysed the data. K.H. wrote the manuscript with feedback from the other authors. K.M., K.F. and Y.N. supervised the project.

The authors declare no competing interests.

APPENDIX A: DETAILED ANALYSIS OF EXPERIMENTAL RESULTS IN SSVQE

In SSVQE, we use the gate-error and measurement-error mitigations. To mitigate gate errors, we scale the effective gate time by a factor of 1, 1.5, and 2, respectively, by adding a necessary delay time to both ends of a control microwave pulse for $R_X(\pi/2)$ and $R_{ZX}(\pi/4)$. We conduct experiments for the three cases. Then, we linearly extrapolate the experimental results to the scale factor of 0 and obtained the mitigated results. Figure 6 shows the experimental results with the gate-error mitigation at the convergence point in SSVQE. The linear extrapolation for the evaluated ground-state energies works well, and the mitigated ground-state energies match theoretical values within the standard deviation. In contrast, except for the case with the atomic distance of 0.1 Å, the evaluated first-excited-state energies are not much affected by the insertion of the delay time. The mitigated first-excited-state energies also deviate slightly from the theoretical values. We guess that the deviation of the first-excited-state energies from the theoretical values originates in a bottleneck for the convergence other than the incoherent error during the pulse sequences. As shown in Fig. 4, while the ground-state energies are well isolated from the other eigenenergies, the first-excited-state energies are close to the second-excited-state energies. Only in the case with the atomic distance of 0.1 Å, the first-excited-state energy is sufficiently isolated from the second-excited-state energy, and thus the gate-error mitigation works well. We conclude that the proximity of the first and the second-excited-state energies slows the convergence of SSVQE, resulting in a slight contamination of the second excited state in the final states.

To mitigate the measurement error, we use a predetermined measurement confusion matrix C. We estimate the true histogram x which minimizes $|y - Cx|^2$ for the measurement histogram y obtained in the experiments. Here, we used SLSQP [80] as an optimizer for the minimization.

Figure 7 shows the experimental traces of the residual errors in SSVQE converging to the low-lying eigenenergies for different atomic distances, where the residual errors almost converge after 36 iterations. Figures 7(a) and 7(b) show the results with and without the gate-error mitigation, respectively. In the mitigated optimization traces, some of the evaluated ground-state energies are less than the true ground-state energies, which is due to the linear extrapolation in the gate-error mitigation. With the averaging of 10^4 times, the shot-noise of each Pauli observable is at most $(1/\sqrt{2})\times 10^{-2} \sim 0.007$. As

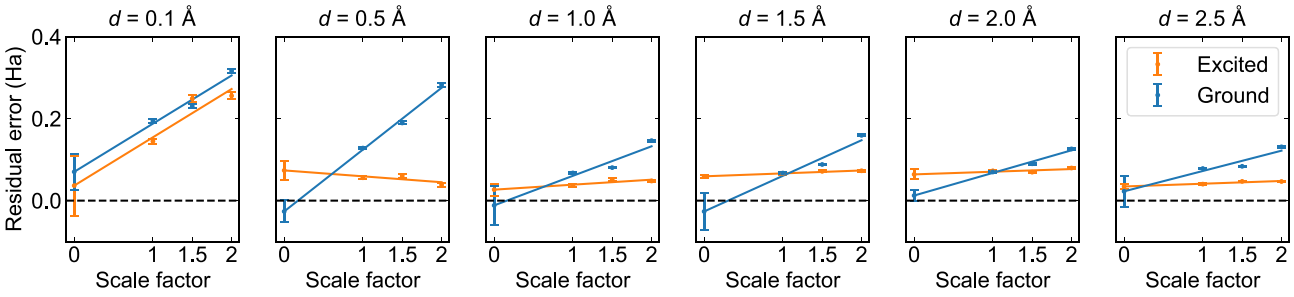

FIG. 6. Gate-error mitigation results of SSVQE after convergence for different atomic distances d. The blue and orange dots represent the residual errors of the ground and first-excited energies, respectively. The horizontal axis represents the scale factor corresponding to the additional delay time for gate-error mitigation. The error bars indicate the standard deviation of the eigenenergies, where the shot number is 10^4.

shown in Fig. 6, the larger error bars mainly arise from the fitting in the linear extrapolation. We also find that the error bar for $d \leqslant 0.5$ Å is larger on average than that for $d \geqslant 1.0$ Å. As mentioned above, the larger error here is mainly due to the fact that the experimental results obtained for the gate-error mitigation no longer follow the linear model, suggesting that the nature of the error in the ansatz circuit has changed.

As shown in Fig. 4, there is a structural transition from a spin singlet to triplet at $d \sim 0.6$ Å, where the first and second excited energies intersect with each other. Here, we summarize coefficients of the Hamiltonian for hydrogen molecule at each atomic distance in Table II. Before and after the transition, low-lying eigenstates differ from each other as follows:

$$|E_0\rangle_{d\leqslant 0.5\,\text{Å}} \sim |01\rangle\,, \tag{A1}$$

$$|E_1\rangle_{d\leqslant 0.5\,\text{Å}} \sim |00\rangle\,, \tag{A2}$$

$$|E_0\rangle_{d\geqslant 1.0\,\text{Å}} \sim |01\rangle\,, \tag{A3}$$

$$|E_1\rangle_{d\geqslant 1.0\,\text{Å}} \sim |10\rangle\,. \tag{A4}$$

Therefore, the maps to be implemented with SSVQE also differ as follows:

$$U_{d\leqslant 0.5\,\text{Å}} \sim |10\rangle\langle 10| + e^{i\delta_1}|00\rangle\langle 01| + U_1^{\perp}, \tag{A5}$$

$$U_{d\geqslant 1.0\,\text{Å}} \sim |10\rangle\langle 10| + e^{i\delta_2}|01\rangle\langle 01| + U_2^{\perp}, \tag{A6}$$

where $\delta_{1,2}$ and $U_{1,2}^{\perp}$ are unknown phase factors and unknown maps between the complementary subspaces, respectively. While $U_{d\geqslant 1.0\,\text{Å}}$ is an identity operator, $U_{d\leqslant 0.5\,\text{Å}}$ is an entangling operation that rotates a qubit according to the state of the other qubit. Therefore, the two $R_{ZX}(\pi/4)$ gates contained in the ansatz circuit need to interfere with each other constructively in the former case and destructively in the latter case. The noise of the ansatz circuit is mainly distributed to the two $R_{ZX}(\pi/4)$ gates, which account for 147 ns of the total duration of the ansatz circuit of 213 ns. Therefore, the change in the constraints imposed on the interference of the two $R_{ZX}(\pi/4)$ gates can significantly change the nature of the circuit noise.

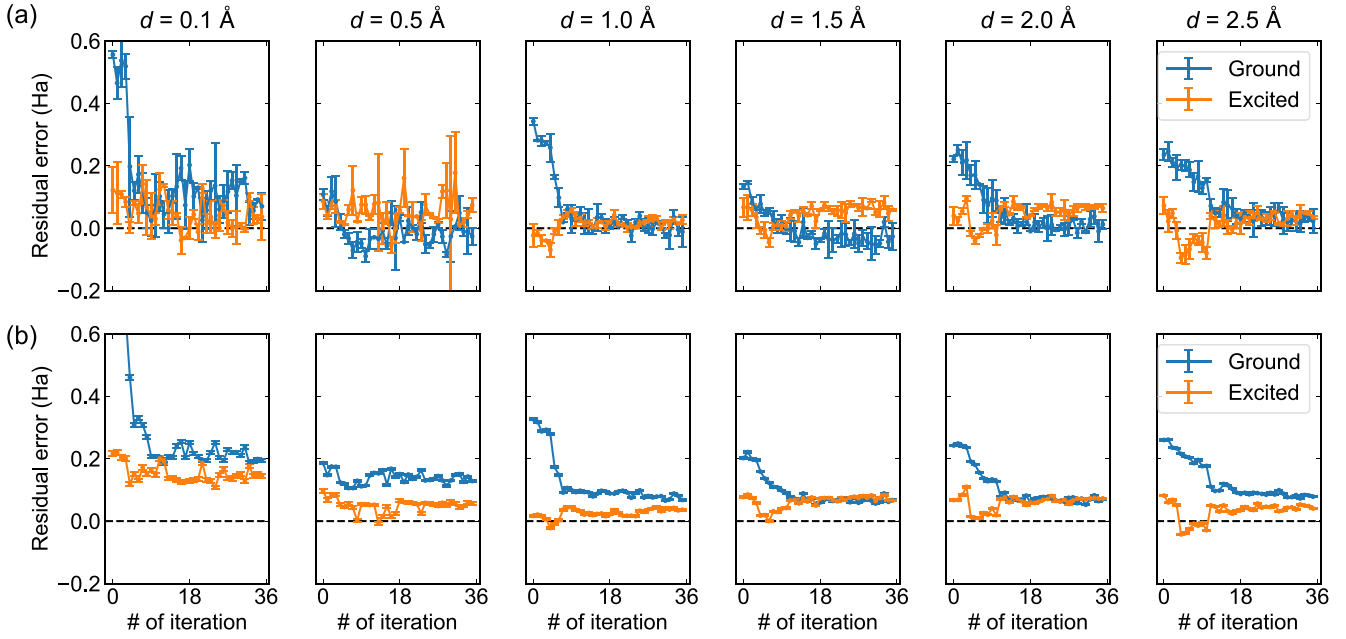

FIG. 7. Optimization traces in SSVQE for different atomic distances d (a) with and (b) without the gate-error mitigation. The raw data in panel (b) are taken at the scale factor of unity. The blue and orange dots represent the residual errors of the ground- and first-excited-state energies, respectively. The error bars indicate the standard deviation of the eigenenergies, where the shot number is 10^4.

TABLE II. List of coefficients $\{c_i\}_{i=0}^{5}$ of the Hamiltonian for hydrogen molecule at each atomic distance d.

d (Å)	c_0 (Ha)	c_1 (Ha)	c_2 (Ha)	c_3 (Ha)	c_4 (Ha)	c_5 (Ha)
0.1	5.46	0.60	−1.45	0.69	0.08	0.08
0.5	0.75	0.43	−0.74	0.62	0.08	0.08
1.0	−0.01	0.27	−0.26	0.52	0.10	0.10
1.5	−0.21	0.19	−0.07	0.44	0.11	0.11
2.0	−0.27	0.13	0.01	0.39	0.13	0.13
2.5	−0.30	0.11	0.05	0.35	0.14	0.14

APPENDIX B: SUBSPACE PROCESS FIDELITY AND SUBSPACE PAULI TRANSFER MATRIX

Process fidelity is a typical measure of the closeness between two quantum processes. The definition of the process fidelity is given as follows:

$$\mathcal{F}(\mathcal{U},\mathcal{V}) \equiv \frac{\mathrm{Tr}[\mathcal{S}_{\mathcal{U}}^{\dagger}\mathcal{S}_{\mathcal{V}}]}{d^2}, \tag{B1}$$

where d is the dimension of the quantum processes, and $S_{\mathcal{U},\mathcal{V}}$ is the superoperator representation on the maps $\mathcal{U}, \mathcal{V}$, respectively. In this subsection, we introduce a new fidelity measure for quantum processes in subspaces, called subspace process fidelity. The subspace process fidelity is defined as follows:

$$\mathcal{F}_{\mathcal{D}_{\mathrm{i}},\mathcal{D}_{\mathrm{o}}}(\mathcal{U},\mathcal{V}) \equiv \mathcal{F}(\mathcal{D}_{\mathrm{o}}\circ\mathcal{U}\circ\mathcal{D}_{\mathrm{i}}, \mathcal{D}_{\mathrm{o}}\circ\mathcal{V}\circ\mathcal{D}_{\mathrm{i}}), \tag{B2}$$

where $\mathcal{D}_{\mathrm{i,o}}$ are the relaxation operators for the input and output subspaces, respectively. To evaluate the subspace time evolution in the low-lying eigensubspace, we introduce the subspace perfect depolarizing channel $\mathcal{D}_{\perp}$ as follows:

$$\mathcal{D}_{\perp}(\rho) = \mathcal{P}_{\parallel}(\rho) + \frac{\mathrm{Tr}[\mathcal{P}_{\perp}(\rho)]}{d_{\perp}} I_{\perp}, \tag{B3}$$

where $\mathcal{P}_{\parallel,\perp}$ are the projection operators on the low-lying eigensubspace and its complementary subspace, respectively, with the dimension $d_{\perp}$ and the identity operator $I_{\perp}$ on the complementary subspace. The subspace process fidelity in the low-lying eigensubspace is calculated as $\mathcal{F}_{\mathcal{D}_{\perp},\mathcal{D}_{\perp}}(\mathcal{U},\mathcal{V})$. The subspace process infidelity in the low-lying eigensubspace is also calculated as $1-\mathcal{F}_{\mathcal{D}_{\perp},\mathcal{D}_{\perp}}(\mathcal{U},\mathcal{V})$. In addition, we introduce the subspace Pauli transfer matrix representation to visualize the properties of the quantum processes in the subspace defined as follows:

$$\mathcal{R}^{\parallel}_{ij} = \frac{\mathrm{Tr}[\sigma_i^{\parallel}\mathcal{T}(t)\sigma_j^{\parallel}]}{d_{\parallel}}, \tag{B4}$$

where $\mathcal{R}^{\parallel}_{ij}$ is the (i,j) element of the subspace Pauli transfer matrix, and $\sigma_i^{\parallel}$ is the ith subspace Pauli operator. For the two-dimensional low-lying eigensubspace of a hydrogen molecule, the subspace Pauli operators are defined as follows:

$$\sigma_0^{\parallel} = |E_0\rangle\langle E_0| + |E_1\rangle\langle E_1|, \tag{B5}$$

$$\sigma_1^{\parallel} = |E_1\rangle\langle E_0| + |E_0\rangle\langle E_1|, \tag{B6}$$

$$\sigma_2^{\parallel} = i(|E_1\rangle\langle E_0| - |E_0\rangle\langle E_1|), \tag{B7}$$

$$\sigma_3^{\parallel} = |E_0\rangle\langle E_0| - |E_1\rangle\langle E_1|, \tag{B8}$$

and $d_{\parallel}=2$ is the dimension of the low-lying eigensubspace. Note that the interaction between the target subspace and the

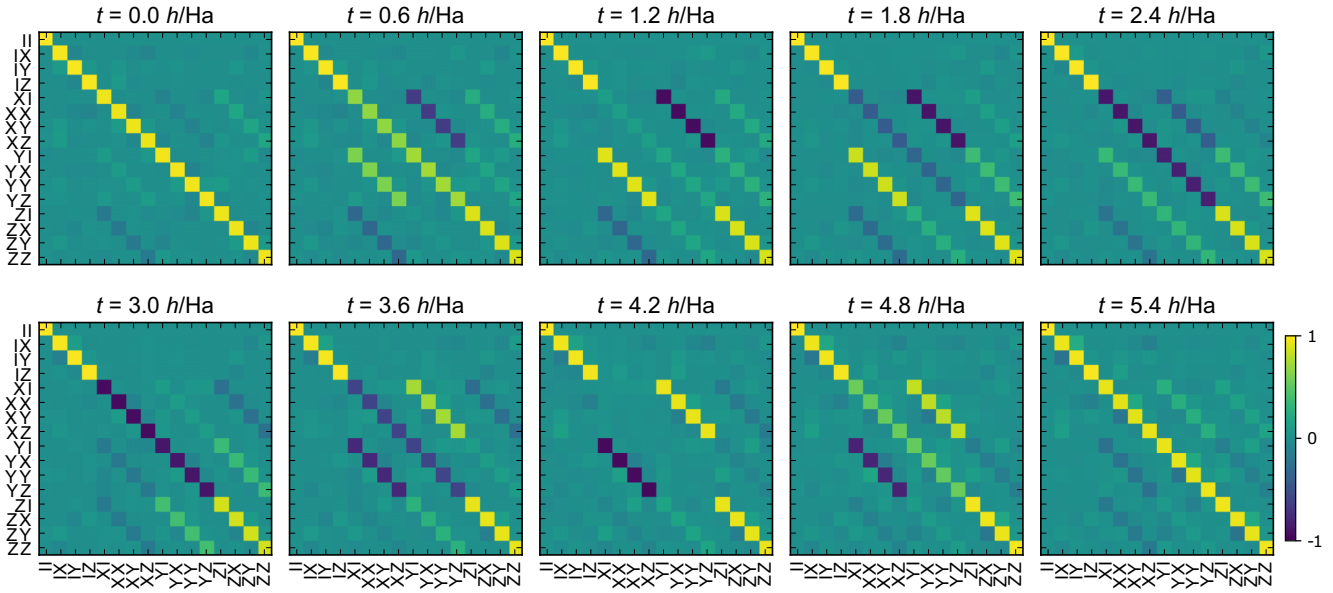

FIG. 8. Experimentally obtained Pauli transfer matrices of the time-evolution operator of a hydrogen molecule mimicked by SVQS for different evolution times t.

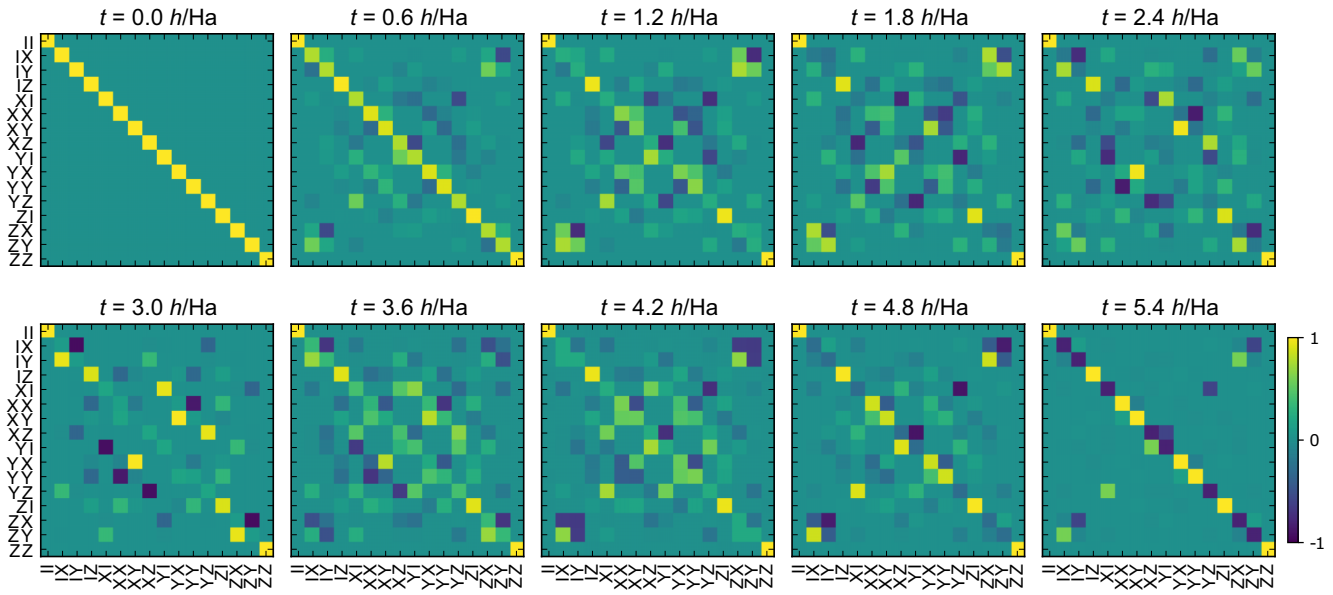

FIG. 9. Numerically obtained Pauli transfer matrices of the time-evolution operator of a hydrogen molecule for different evolution times t.

complementary subspace is regarded as the leakage, and the obtained subspace Pauli transfer matrix generally does not preserve the trace of the system. In the low-lying eigensubspace, the Hamiltonian of a hydrogen molecule is given as follows:

$$\mathcal{H}^{\parallel} = E_0 \left|E_0\right\rangle \left\langle E_0\right| + E_1 \left|E_1\right\rangle \left\langle E_1\right| \tag{B9}$$

$$= \frac{E_0 + E_1}{2}\sigma_0^{\parallel} + \frac{E_0 - E_1}{2}\sigma_3^{\parallel}. \tag{B10}$$

Therefore, the subspace time-evolution operator corresponds to a phase rotation gate in the low-lying eigensubspace as follows:

$$\mathcal{T}^{\parallel}(t) = \exp\left\{-i\left(\frac{E_0 - E_1}{2}t\right)\sigma_3^{\parallel}\right\}. \tag{B11}$$

APPENDIX C: DETAILED ANALYSIS OF EXPERIMENTAL RESULTS IN SVQS

The experimentally obtained Pauli transfer matrices of the subspace time-evolution operator mimicked by SVQS are shown in Fig. 8. The Pauli transfer matrices are estimated from the gate-error-mitigated results with the maximum likelihood estimation using the predetermined initial thermal populations and measurement confusion matrix, which is supported by a quantum characterization toolkit, Quara [70]. Figure 9 shows the theoretical Pauli transfer matrices of the ideal time-evolution operator. At first glance, the Pauli transfer matrices shown in Figs. 8 and 9 look totally different. This is because SVQS mimics only the subspace time-evolution operator within the low-lying eigensubspace $\mathcal{S}_{\parallel}$. Therefore, for a proper comparison, we extract the subspace Pauli transfer matrices of the time-evolution operators in the low-lying eigensubspace defined in Eq. (B4). Figure 5 shows the numerically and experimentally obtained subspace Pauli transfer matrices of the time-evolution operator in the low-lying eigensubspace $\mathcal{S}_{\parallel}$ for different evolution times t. From the subspace Pauli transfer matrices, we can estimate the Hamiltonian mimicked by SVQS. Here, we use the dynamics generator analysis [81] to extract unitary components from the quantum processes. For the extracted unitary components, we numerically search for the approximate Hamiltonian of subspace time-evolution operator mimicked by SVQS with Powell method [82]. The ideal and fitted Hamiltonian in the low-lying eigensubspace is written as follows:

$$\mathcal{H}_{\text{ideal}}^{\parallel} \sim +0.00\sigma_1^{\parallel} + 0.00\sigma_2^{\parallel} - 0.57\sigma_3^{\parallel}, \tag{C1}$$

$$\mathcal{H}_{\text{fit}}^{\parallel} \sim -0.19\sigma_1^{\parallel} + 0.01\sigma_2^{\parallel} - 0.54\sigma_3^{\parallel}. \tag{C2}$$

The fitted Hamiltonian approximates the unitary components of the subspace time evolution with a process fidelity of 0.998(1). From the fitted Hamiltonian, we find that the time evolution mimicked by SVQS has a rotation-speed error of 1.1% and a rotation-axis error of 19.3°.

[1] E. Runge and E. K. U. Gross, Density-Functional Theory for Time-Dependent Systems, Phys. Rev. Lett. **52**, 997 (1984).
[2] R. P. Feynman, Simulating physics with computers, Int. J. Theor. Phys. **21**, 467 (1982).
[3] I. M. Georgescu, S. Ashhab, and F. Nori, Quantum simulation, Rev. Mod. Phys. **86**, 153 (2014).
[4] S. Lloyd, Universal quantum simulators, Science **273**, 1073 (1996).

[5] N. Wiebe, D. W. Berry, P. Høyer, and B. C. Sanders, Simulating quantum dynamics on a quantum computer, J. Phys. A: Math. Theor. **44**, 445308 (2011).

[6] D. Poulin, A. Qarry, R. Somma, and F. Verstraete, Quantum Simulation of Time-Dependent Hamiltonians and the Convenient Illusion of Hilbert Space, Phys. Rev. Lett. **106**, 170501 (2011).

[7] A. M. Childs and N. Wiebe, Hamiltonian simulation using linear combinations of unitary operations, Quantum Inf. Comput. **12**, 901 (2012).

[8] K. Seki and S. Yunoki, Quantum power method by a superposition of time-evolved states, PRX Quantum **2**, 010333 (2021).

[9] D. W. Berry, A. M. Childs, R. Cleve, R. Kothari, and R. D. Somma, Simulating Hamiltonian Dynamics with a Truncated Taylor Series, Phys. Rev. Lett. **114**, 090502 (2015).

[10] D. W. Berry, A. M. Childs, Y. Su, X. Wang, and N. Wiebe, Time-dependent Hamiltonian simulation with L^1-norm scaling, Quantum **4**, 254 (2020).

[11] E. Campbell, Random Compiler for Fast Hamiltonian Simulation, Phys. Rev. Lett. **123**, 070503 (2019).

[12] G. H. Low and I. L. Chuang, Optimal Hamiltonian Simulation by Quantum Signal Processing, Phys. Rev. Lett. **118**, 010501 (2017).

[13] S. B. Bravyi and A. Y. Kitaev, Quantum codes on a lattice with boundary, arXiv:quant-ph/9811052.

[14] A. G. Fowler, M. Mariantoni, J. M. Martinis, and A. N. Cleland, Surface codes: Towards practical large-scale quantum computation, Phys. Rev. A **86**, 032324 (2012).

[15] S. Boixo, S. V. Isakov, V. N. Smelyanskiy, R. Babbush, N. Ding, Z. Jiang, M. J. Bremner, J. M. Martinis, and H. Neven, Characterizing quantum supremacy in near-term devices, Nat. Phys. **14**, 595 (2018).

[16] A. Bouland, B. Fefferman, C. Nirkhe, and U. Vazirani, On the complexity and verification of quantum random circuit sampling, Nat. Phys. **15**, 159 (2018).

[17] J. Chen, F. Zhang, C. Huang, M. Newman, and Y. Shi, Classical simulation of intermediate-size quantum circuits (2018), arXiv:1805.01450.

[18] M. Cerezo, A. Arrasmith, R. Babbush, S. C. Benjamin, S. Endo, K. Fujii, J. R. McClean, K. Mitarai, X. Yuan, L. Cincio *et al.*, Variational quantum algorithms, Nat. Rev. Phys. **3**, 625 (2021).

[19] A. Peruzzo, J. McClean, P. Shadbolt, M.-H. Yung, X.-Q. Zhou, P. J. Love, A. Aspuru-Guzik, and J. L. O'brien, A variational eigenvalue solver on a photonic quantum processor, Nat. Commun. **5**, 4213 (2014).

[20] J. R. McClean, J. Romero, R. Babbush, and A. Aspuru-Guzik, The theory of variational hybrid quantum-classical algorithms, New J. Phys. **18**, 023023 (2016).

[21] B. Bauer, D. Wecker, A. J. Millis, M. B. Hastings, and M. Troyer, Hybrid Quantum-Classical Approach to Correlated Materials, Phys. Rev. X **6**, 031045 (2016).

[22] A. Kandala, A. Mezzacapo, K. Temme, M. Takita, M. Brink, J. M. Chow, and J. M. Gambetta, Hardware-efficient variational quantum eigensolver for small molecules and quantum magnets, Nature (London) **549**, 242 (2017).

[23] Y. Li and S. C. Benjamin, Efficient Variational Quantum Simulator Incorporating Active Error Minimization, Phys. Rev. X **7**, 021050 (2017).

[24] X. Yuan, S. Endo, Q. Zhao, Y. Li, and S. C. Benjamin, Theory of variational quantum simulation, Quantum **3**, 191 (2019).

[25] S. Endo, J. Sun, Y. Li, S. C. Benjamin, and X. Yuan, Variational Quantum Simulation of General Processes, Phys. Rev. Lett. **125**, 010501 (2020).

[26] S. McArdle, T. Jones, S. Endo, Y. Li, S. C. Benjamin, and X. Yuan, Variational ansatz-based quantum simulation of imaginary time evolution, npj Quantum Inf. **5**, 75 (2019).

[27] C. Cîrstoiu, Z. Holmes, J. Iosue, L. Cincio, P. J. Coles, and A. Sornborger, Variational fast forwarding for quantum simulation beyond the coherence time, npj Quantum Inf. **6**, 82 (2020).

[28] M. Otten, C. L. Cortes, and S. K. Gray, Noise-resilient quantum dynamics using symmetry-preserving ansatzes, arXiv:1910.06284.

[29] B. Commeau, M. Cerezo, Z. Holmes, L. Cincio, P. J. Coles, and A. Sornborger, Variational Hamiltonian diagonalization for dynamical quantum simulation, arXiv:2009.02559.

[30] J. Gibbs, K. Gili, Z. Holmes, B. Commeau, A. Arrasmith, L. Cincio, P. J. Coles, and A. Sornborger, Long-time simulations with high fidelity on quantum hardware, arXiv:2102.04313.

[31] K. M. Nakanishi, K. Mitarai, and K. Fujii, Subspace-search variational quantum eigensolver for excited states, Phys. Rev. Res. **1**, 033062 (2019).

[32] J. R. McClean, M. E. Kimchi-Schwartz, J. Carter, and W. A. de Jong, Hybrid quantum-classical hierarchy for mitigation of decoherence and determination of excited states, Phys. Rev. A **95**, 042308 (2017).

[33] J. R. McClean, Z. Jiang, N. C. Rubin, R. Babbush, and H. Neven, Decoding quantum errors with subspace expansions, Nat. Commun. **11**, 636 (2020).

[34] T. Takeshita, N. C. Rubin, Z. Jiang, E. Lee, R. Babbush, and J. R. McClean, Increasing the Representation Accuracy of Quantum Simulations of Chemistry without Extra Quantum Resources, Phys. Rev. X **10**, 011004 (2020).

[35] P. Jordan and E. Wigner, Über das paulische Äquivalenzverbot, Z. Phys. **47**, 631 (1928).

[36] S. B. Bravyi and A. Y. Kitaev, Fermionic quantum computation, Ann. Phys. **298**, 210 (2002).

[37] D. C. McKay, C. J. Wood, S. Sheldon, J. M. Chow, and J. M. Gambetta, Efficient z gates for quantum computing, Phys. Rev. A **96**, 022330 (2017).

[38] V. Bonch-Bruevich, S. Tyablikov, and R. J. Seeger, The green function method in statistical mechanics, Am. J. Phys. **33**, 597 (1965).

[39] A. A. Abrikosov, L. P. Gorkov, I. Dzyaloshinski, R. A. Silverman, and G. H. Weiss, Methods of quantum field theory in statistical physics, Phys. Today **17**, 78 (1964).

[40] K. Hashimoto, K. Murata, and R. Yoshii, Out-of-time-order correlators in quantum mechanics, J. High Energy Phys. 10 (2017) 138.

[41] A. Wisniacki, Loschmidt echo, Scholarpedia **7**, 11687 (2012).

[42] S. Tamate, Y. Tabuchi, L. Szikszai, K. Kusuyama, K. Zuo, Z. Yan, A. Badrutdinov, Y. Hishida, W. Qiu, H. Terai, G. Fujii, K. Makise, N. Watanabe, H. Nakagawa, M. Fujino, M. Ukibe, W. Mizubayashi, K. Kikuchi, and Y. Nakamura, Scalable packaging design for large-scale superconducting quantum circuit, Bull. Am. Phys. Soc. **66**, C30.9 (2021).

[43] E. Lucero, J. Kelly, R. C. Bialczak, M. Lenander, M. Mariantoni, M. Neeley, A. D. O'Connell, D. Sank, H. Wang, M. Weides, J. Wenner, T. Yamamoto, A. N. Cleland, and J. M. Martinis, Reduced phase error through optimized control of a superconducting qubit, Phys. Rev. A **82**, 042339 (2010).

[44] J. M. Gambetta, A. D. Córcoles, S. T. Merkel, B. R. Johnson, J. A. Smolin, J. M. Chow, C. A. Ryan, C. Rigetti, S. Poletto, T. A. Ohki, M. B. Ketchen, and M. Steffen, Characterization of Addressability by Simultaneous Randomized Benchmarking, Phys. Rev. Lett. **109**, 240504 (2012).

[45] C. Rigetti and M. Devoret, Fully microwave-tunable universal gates in superconducting qubits with linear couplings and fixed transition frequencies, Phys. Rev. B **81**, 134507 (2010).

[46] J. M. Chow, A. D. Córcoles, J. M. Gambetta, C. Rigetti, B. R. Johnson, J. A. Smolin, J. R. Rozen, G. A. Keefe, M. B. Rothwell, M. B. Ketchen, and M. Steffen, Simple All-Microwave Entangling Gate for Fixed-Frequency Superconducting Qubits, Phys. Rev. Lett. **107**, 080502 (2011).

[47] E. Magesan, J. M. Gambetta, B. R. Johnson, C. A. Ryan, J. M. Chow, S. T. Merkel, M. P. da Silva, G. A. Keefe, M. B. Rothwell, T. A. Ohki, M. B. Ketchen, and M. Steffen, Efficient Measurement of Quantum Gate Error by Interleaved Randomized Benchmarking, Phys. Rev. Lett. **109**, 080505 (2012).

[48] P. Watts, M. O'Connor, and J. Vala, Metric structure of the space of two-qubit gates, perfect entanglers and quantum control, Entropy **15**, 1963 (2013).

[49] A. Blais, R.-S. Huang, A. Wallraff, S. M. Girvin, and R. J. Schoelkopf, Cavity quantum electrodynamics for superconducting electrical circuits: An architecture for quantum computation, Phys. Rev. A **69**, 062320 (2004).

[50] A. Wallraff, D. I. Schuster, A. Blais, L. Frunzio, J. Majer, M. H. Devoret, S. M. Girvin, and R. J. Schoelkopf, Approaching Unit Visibility for Control of a Superconducting Qubit with Dispersive Readout, Phys. Rev. Lett. **95**, 060501 (2005).

[51] E. Jeffrey, D. Sank, J. Y. Mutus, T. C. White, J. Kelly, R. Barends, Y. Chen, Z. Chen, B. Chiaro, A. Dunsworth, A. Megrant, P. J. J. O'Malley, C. Neill, P. Roushan, A. Vainsencher, J. Wenner, A. N. Cleland, and J. M. Martinis, Fast Accurate State Measurement with Superconducting Qubits, Phys. Rev. Lett. **112**, 190504 (2014).

[52] E. A. Sete, J. M. Martinis, and A. N. Korotkov, Quantum theory of a bandpass Purcell filter for qubit readout, Phys. Rev. A **92**, 012325 (2015).

[53] J. Y. Mutus, T. C. White, R. Barends, Y. Chen, Z. Chen, B. Chiaro, A. Dunsworth, E. Jeffrey, J. Kelly, A. Megrant, C. Neill, P. J. J. O'Malley, P. Roushan, D. Sank, A. Vainsencher, J. Wenner, K. M. Sundqvist, A. N. Cleland, and J. M. Martinis, Strong environmental coupling in a Josephson parametric amplifier, Appl. Phys. Lett. **104**, 263513 (2014).

[54] Y. Urade, K. Zuo, S. Baba, C. Chang, K.-I. Nittoh, K. Inomata, Z. Lin, T. Yamamoto, and Y. Nakamura, Flux-driven impedance-matched Josephson parametric amplifier with improved pump efficiency, Bull. Am. Phys. Soc. **66**, A28.10 (2021).

[55] P. J. J. O'Malley, R. Babbush, I. D. Kivlichan, J. Romero, J. R. McClean, R. Barends, J. Kelly, P. Roushan, A. Tranter, N. Ding, B. Campbell, Y. Chen, Z. Chen, B. Chiaro, A. Dunsworth, A. G. Fowler, E. Jeffrey, E. Lucero, A. Megrant, J. Y. Mutus, M. Neeley, C. Neill, C. Quintana, D. Sank, A. Vainsencher, J. Wenner, T. C. White, P. V. Coveney, P. J. Love, H. Neven, A. Aspuru-Guzik, and J. M. Martinis, Scalable Quantum Simulation of Molecular Energies, Phys. Rev. X **6**, 031007 (2016).

[56] J. R. McClean, K. J. Sung, I. D. Kivlichan, Y. Cao, C. Dai, E. S. Fried, C. Gidney, B. Gimby, P. Gokhale, T. Häner, T. Hardikar, V. Havlíček, O. Higgott, C. Huang, J. Izaac, Z. Jiang, X. Liu, S. McArdle, M. Neeley, T. O'Brien, B. O'Gorman, I. Ozfidan, M. D. Radin, J. Romero, N. Rubin, N. P. D. Sawaya, K. Setia, S. Sim, D. S. Steiger, M. Steudtner, Q. Sun, W. Sun, D. Wang, F. Zhang, and R. Babbush, Openfermion: The electronic structure package for quantum computers, arXiv:1710.07629.

[57] R. M. Parrish, L. A. Burns, D. G. A. Smith, A. C. Simmonett, A. E. DePrince, E. G. Hohenstein, U. Bozkaya, A. Y. Sokolov, R. Di Remigio, R. M. Richard, J. F. Gonthier, A. M. James, H. R. McAlexander, A. Kumar, M. Saitow, X. Wang, B. P. Pritchard, P. Verma, H. F. Schaefer, K. Patkowski, R. A. King, E. F. Valeev, F. A. Evangelista, J. M. Turney, T. D. Crawford, and C. D. Sherrill, Psi4 1.1: An open-source electronic structure program emphasizing automation, advanced libraries, and interoperability, J. Chem. Theory Comput. **13**, 3185 (2017).

[58] T.-C. Yen, V. Verteletskyi, and A. F. Izmaylov, Measuring all compatible operators in one series of single-qubit measurements using unitary transformations, J. Chem. Theory Comput. **16**, 2400 (2020).

[59] A. Jena, S. Genin, and M. Mosca, Pauli partitioning with respect to gate sets, arXiv:1907.07859.

[60] V. Verteletskyi, T.-C. Yen, and A. F. Izmaylov, Measurement optimization in the variational quantum eigensolver using a minimum clique cover, J. Chem. Phys. **152**, 124114 (2020).

[61] P. Gokhale, O. Angiuli, Y. Ding, K. Gui, T. Tomesh, M. Suchara, M. Martonosi, and F. T. Chong, Minimizing state preparations in variational quantum eigensolver by partitioning into commuting families, arXiv:1907.13623.

[62] O. Crawford, B. van Straaten, D. Wang, T. Parks, E. Campbell, and S. Brierley, Efficient quantum measurement of Pauli operators in the presence of finite sampling error, Quantum **5**, 385 (2021).

[63] K. Temme, S. Bravyi, and J. M. Gambetta, Error Mitigation for Short-Depth Quantum Circuits, Phys. Rev. Lett. **119**, 180509 (2017).

[64] S. Endo, Z. Cai, S. C. Benjamin, and X. Yuan, Hybrid quantum-classical algorithms and quantum error mitigation, J. Phys. Soc. Jpn. **90**, 032001 (2021).

[65] F. B. Maciejewski, Z. Zimborás, and M. Oszmaniec, Mitigation of readout noise in near-term quantum devices by classical post-processing based on detector tomography, Quantum **4**, 257 (2020).

[66] Y. Chen, M. Farahzad, S. Yoo, and T.-C. Wei, Detector tomography on IBM quantum computers and mitigation of an imperfect measurement, Phys. Rev. A **100**, 052315 (2019).

[67] H. Kwon and J. Bae, A hybrid quantum-classical approach to mitigating measurement errors in quantum algorithms, IEEE Trans. Comput. **70**, 1401 (2021).

[68] K. M. Nakanishi, K. Fujii, and S. Todo, Sequential minimal optimization for quantum-classical hybrid algorithms, Phys. Rev. Res. **2**, 043158 (2020).

[69] M. Mohseni, A. T. Rezakhani, and D. A. Lidar, Quantum-process tomography: Resource analysis of different strategies, Phys. Rev. A **77**, 032322 (2008).

[70] T. Sugiyama, Quara: An open-source software for quantum characterization, https://quara.readthedocs.io/en/stable/.

[71] N. Yoshioka, Y. O. Nakagawa, Y. Ohnishi, and W. Mizukami, Variational quantum simulation for periodic materials, arXiv:2008.09492.

[72] X. Yuan, J. Sun, J. Liu, Q. Zhao, and Y. Zhou, Quantum Simulation with Hybrid Tensor Networks, Phys. Rev. Lett. **127**, 040501 (2021).

[73] K. Fujii, K. Mitarai, W. Mizukami, and Y. O. Nakagawa, Deep variational quantum eigensolver: A divide-and-conquer method for solving a larger problem with smaller size quantum computers, arXiv:2007.10917.

[74] C. Cao, J. Hu, W. Zhang, X. Xu, D. Chen, F. Yu, J. Li, H. Hu, D. Lv, and M.-H. Yung, Towards a larger molecular simulation on the quantum computer: Up to 28 qubits systems accelerated by point group symmetry, arXiv:2109.02110.

[75] K. Yamamoto, D. Z. Manrique, I. Khan, H. Sawada, and D. M. Ramo, Quantum hardware calculations of periodic systems: Hydrogen chain and iron crystals, arXiv:2109.08401.

[76] A. Luis and J. Peřina, Optimum phase-shift estimation and the quantum description of the phase difference, Phys. Rev. A **54**, 4564 (1996).

[77] R. Cleve, A. Ekert, C. Macchiavello, and M. Mosca, Quantum algorithms revisited, Proc. Math. Phys. Eng. Sci. **454**, 339 (1998).

[78] V. Bužek, R. Derka, and S. Massar, Optimal Quantum Clocks, Phys. Rev. Lett. **82**, 2207 (1999).

[79] A. W. Harrow, A. Hassidim, and S. Lloyd, Quantum Algorithm for Linear Systems of Equations, Phys. Rev. Lett. **103**, 150502 (2009).

[80] P. Virtanen, R. Gommers, T. E. Oliphant, M. Haberland, T. Reddy, D. Cournapeau, E. Burovski, P. Peterson, W. Weckesser, J. Bright, S. J. van der Walt, M. Brett, J. Wilson, K. J. Millman, N. Mayorov, A. R. J. Nelson, E. Jones, R. Kern, E. Larson, C J Carey, İ. Polat, Y. Feng, E. W. Moore, J. VanderPlas, D. Laxalde, J. Perktold, R. Cimrman, I. Henriksen, E. A. Quintero, C. R. Harris, A. M. Archibald, A. H. Ribeiro, F. Pedregosa, P. van Mulbregt, and SciPy 1.0 Contributors, SciPy 1.0: Fundamental algorithms for scientific computing in Python, Nat. Methods **17**, 261 (2020).

[81] T. Sugiyama, S. Imori, and F. Tanaka, Self-consistent quantum tomography with regularization, Phys. Rev. A **103**, 062615 (2021).

[82] M. J. D. Powell, An efficient method for finding the minimum of a function of several variables without calculating derivatives, Comput. J. **7**, 155 (1964).